PNAS
www.pnas.org

Supplementary Information for
Visualizing β-adrenergic receptor dynamics and differential localization in cardiomyocytes

Marc Bathe-Peters[#], Philipp Gmach[#], Horst-Holger Boltz, Jürgen Einsiedel, Michael Gotthardt, Harald Hübner, Peter Gmeiner, Martin J. Lohse*, Paolo Annibale*

Corresponding authors: Paolo Annibale and Martin J. Lohse
Email m.lohse@mdc-berlin.de, paolo.annibale@mdc-berlin.de

This PDF file includes:

Supplementary Text
Synthesis Scheme S1
Supplementary Materials and Methods
SI References
SI Figures 1-8

Other supplementary materials for this manuscript include the following:

Supplementary Information Text

Chemical Synthesis

The synthesis of the fluorescent ligand **I1319** was performed starting from the chiral epoxide **2** (1, 2), which was prepared by an S_N2-reaction of 4-hydroxy-9*H*-carbazole (**1**) with (*S*)-glycidyl 3-nitrobenzenesulfonate (Scheme S1). Fmoc protection of 2-(4-nitrophenyl)ethylamine (**3**) to give the intermediate **4** and subsequent reduction of the nitro group resulted in the formation of the primary aromatic amine **5** (3, 4). Acylation of **5** with hexynoic acid in presence of *N*-ethyl-*N'*-(3-dimethylaminopropyl)carbodiimide hydrochloride (EDC-HCl) and 1-hydroxy-7-azabenzotriazole (HOAt) gave the anilide derivative **6**, which was deprotected in presence of 1,8-diazabicyclo[5.4.0]undec-7-ene (DBU) to furnish the primary amine **7**. **7** was subjected to a nucleophilic ring opening reaction of the epoxide derivative **2** to obtain the alkyne **8**. Investigation of **8** by chiral HPLC in comparison with a racemic mixture (**rac-8**, synthesized analogously from the racemic epoxide derivative **rac-2**) indicated 98.2% enantiomeric purity and, thus, the stereochemical integrity of the protocol. Finally, copper(I)-catalyzed azide-alkyne cycloaddition (CuAAC) (5) with the Alexa Fluor 647 derivative AF 647 azide (Jena Bioscience) employing the chelator tris((1-(3-hydroxypropyl)-1*H*-1,2,3-triazol-4-yl)methyl)amine (THPTA) under aqueous, buffered conditions (pH 7.5) gave access to the fluorescent ligand **JE1319**.

Synthesis Scheme

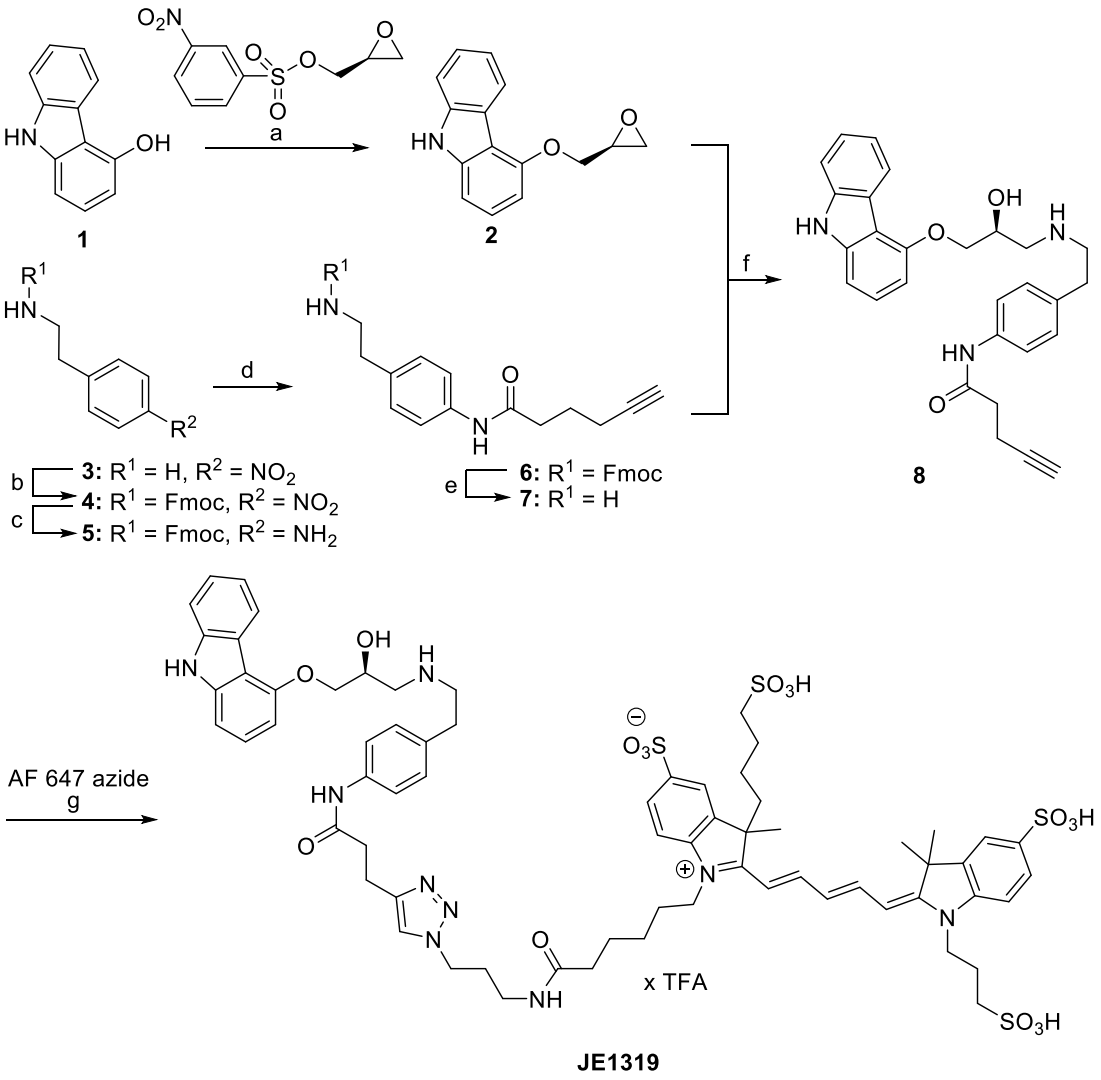

Scheme S1. Reagents and conditions: Synthesis of the fluorescent ligand **JE1319**, reagents and conditions: (a) 1. NaH, DMF, 0 °C, 30 min, 2. (*S*)-glycidyl 3-nitrobenzenesulfonate, DMF, rt, 23 h, (66%); (b) Fmoc-Cl, DIEA, CH_2Cl_2 0 °C -> rt, 3 h (66%); (c) $SnCl_2$ × 2 H_2O, DMF, rt, 16 h (82%); (d) hexynoic acid, EDC × HCl, HOAt, CH_2Cl_2, DMF, rt, 2 h (69%); (e) DBU, DMF, rt, 2 h (70%); (f) iPrOH, 85 °C, 5 h (86%); (g) $CuSO_4$ × 5 H_2O, THPTA, sodium ascorbate, HEPES buffer pH 7.5, MeOH, rt, 10 min (50%).

Supplementary Materials and Methods

Animal models and procedures

The following mouse models were used throughout the study:

Name	Genotype	Background
β_1-AR-TG4	TG/wt	FVB/N
β_2-AR-TG32	TG/wt	FVB/N
wt	wt/wt	FVB/N
β_1-AR/β_2-AR-k.o.	-/-	mixed background

Cardiomyocyte isolation buffers
All required buffers including the perfusion buffer (AfCS Solution Protocol PS00000451), myocyte digestion buffer (MC digestion buffer, AfCS Solution Protocol PS00000447), myocyte stopping buffers (MC stop 1, AfCS Solution Protocol PS00000449 and MC stop 2, AfCS Solution Protocol PS00000450), myocyte plating medium (MC plating medium, AfCS Solution Protocol PS00000448) and myocyte culture medium (MC culture medium, AfCS Solution Protocol PS00000446), were generated as described in the AfCS protocols and prepared freshly for each experimental day. A few modifications to the buffer formulations were made. The MC digestion buffer was prepared with Liberase DH (Roche) instead of Liberase blendzyme 1 (Roche). Furthermore, a phenol red-free Minimum Essential Medium (MEM) with Earle's salts (Gibco) instead of Hank's salts was used as a basis for the MC culture and MC plating medium. Lastly, the MC culture medium was supplemented with standard bovine serum albumin (BSA) (Sigma Aldrich) instead of myocyte BSA, and the MC plating as well as MC stop1 and MC stop2 media were produced using fetal bovine serum (FBS) (Sigma-Aldrich) instead of bovine calf serum (BCS), respectively.

CM-hiPSC culture and differentiation
In short, hiPSC were cultured in essential 8 basal medium (E8 medium) (Gibco) on Geltrex- (Gibco) coated plates 4 days prior to cardiac induction. As soon as they reached 80-90% confluency, mesodermal differentiation was induced on day 0 for 24 h by changing the medium to cardiac priming medium composed of RPMI 1640 (Gibco), 1x B27 supplement without insulin (Gibco) and 6 µM CHIR99021 (Sellek Chem). On the following day basal differentiation medium (cardiac priming medium without CHIR99021) was added on top of the old cardiac priming medium. Cardiogenesis was induced on day 3 by changing the medium to basal differentiation medium supplemented with 5 µM of the Wnt inhibitor IWR-1 (Sellek Chem). On day 5, without removing the old medium, basal differentiation medium was added to let cells grow for 2 more days. From day 7 onwards, cells were cultured in maintenance medium (RPMI 1640, B27 with insulin (Gibco)) which was exchanged every 3 days. On day 9, cells were selected for cardiomyocytes over 4 days in RPMI 1640 without glucose (Gibco) supplemented with CDM3 supplement (Sigma Aldrich) and 5 mM sodium DL-lactate (Sigma Aldrich). The beating CM-hiPSCs were then cultured in maintenance medium which was exchanged every 3-5 days. Three days prior to imaging CM-hiPSC were detached as single cells and seeded in Geltrex-coated µ-slides (Ibidi). Until the day of experiment CM-hiPSC were cultured in maintenance medium with 3 µM CHIR99021 and 1x RevitaCell supplement (Life Technologies).

Fluorescence plate reader analysis
HEK293AD cells were transfected with cDNA encoding for the indicated receptors. One day later, cells were seeded in dark-bottom 96-well plates (Sarsted) at a seeding density of 75,000 cells/well. Two days after transfection cells were incubated for 60 minutes with increasing concentrations of JE1319 at 37°C. Non-specific binding was determined in the presence and by preincubating cells for 60 minutes with 100 µM propranolol, and subtracted from the non-preincubated values, at each

concentration. Prior to measurement in a Neo2 multimode Plate Reader (BioTek), cells were washed four times in imaging buffer, as described in the Materials and Methods. Fluorescence of JE1319 was excited at 640/20 nm and collected at 690/40 nm. Differences in expression levels and seeded cell numbers were accounted for by normalization to the fluorescence of the respective receptor tag excited at 430/30 nm and collected at 490/30 nm. The saturation curves for specific JE1319 binding on intact HEK293AD cells were analyzed by nonlinear regression using the algorithms ("one site specific binding") implemented in PRISM 8.0 (GraphPad Software, San Diego, CA) to calculate K_d values.

Analysis of confocal linescans

Single pixel autocorrelation

In the first approach, temporal autocorrelation in each pixel of the linescan was calculated. The FCS analysis of the recorded kymographs or linescans was custom implemented in MATLAB to enhance the analysis with an artifact control. **Figure S2** illustrates how the analysis is conducted along the plasma membrane. The first step is a selection of a ROI in a cell, here a β_1-AR-TG4 CM incubated with 5 nM JE1319, in which the line scan is performed (A). This line is repeatedly scanned over time which leads to an image like in panel B. Here, for representation purposes, but not the analysis multiple time points are averaged together (shown are 500 time points). The analysis includes a bleaching correction via a moving average (6) and a high pass filtering by dividing the total series into smaller sections of about 36 s length (temporal filtering). For each scan the first 2^{17} lines, where photobleaching is most prominent, are cut off to reduce the influence of the slow-timescale bleaching fluctuation from the autocorrelation analysis. In case the scans are performed across TTs either spatial filtering around the tubules is performed to analyze only the relevant locations (overexpression) or the entire spatial line was analyzed (across TTs in wt and k.o. cells). Panel C shows the calculated autocorrelations for each pixel. Each row represents the autocorrelations from one pixel in one of the temporal sections. Depending on the length of the scan multiple temporal sections were created. Panel C illustrates the removal of correlations with artifacts or from artifacts. From the remaining correlations an average autocorrelation is derived over space (panel D). This includes the correlations from all the temporal sections.

FCS compares statistical fluctuations of fluorescent particles in the effective detection volume to extract information on equilibrium processes in the sample (7). In line-scan FCS, which is applied in this work, the statistical accuracy and thus the accuracy of diffusion measurements improves due to the increased sampling arising from measuring multiple pixels within one line (8). From the recorded time-trace of fluorescent intensity in the effective detection volume an autocorrelation G(τ) which reflects the time-scale of the fluorescence intensity fluctuations can be calculated according to the following formula:

$$G(\tau) = \frac{\langle I(t) \cdot I(t+\tau) \rangle}{\langle I(t) \rangle^2}$$

The pointed brackets represent an averaging over all time values t (9). The autocorrelation function G(τ) is then fit to theoretical models usually derived by approximating the Gaussian intensity profile. In this work diffusion occurs on membranes, hence the autocorrelation function will be fit to the customary two dimensional (2D) formula (10). In a T-tubule with a radius smaller than the beam waist, diffusion appears (**Figure S3**) to be fit adequately with a one dimensional (1D) model (11). If we additionally consider photophysical processes such as blinking of the dye, the following equations are derived (10):

$$\textbf{2D}: G_{2D}(\tau) = \frac{1}{N} \frac{1}{1+\frac{4D\tau}{\omega_0^2}} \left(\frac{1-T+T \cdot e^{-\frac{\tau}{\tau_T}}}{1-T} \right) + G_\infty$$

$$\textbf{1D}: G_{1D}(\tau) = \frac{1}{N}\frac{1}{\sqrt{1+\frac{4D\tau}{\omega_0^2}}}\left(\frac{1-T+T\cdot e^{-\frac{\tau}{\tau_T}}}{1-T}\right) + G_\infty$$

In which ω_0 is the radial beam radius describing the extent of the radial distance in the focal plane at $I(R,Z)/I_0 = e^{-2}$, D the diffusion constant, N the number of particles, τ the temporal time lag and G_∞ the limiting value of $G(\tau)$ for $\tau \rightarrow \infty$ (7).

The photophysical process is described by τ_T is the lifetime of the blinking process and T the fraction of the molecules in this process. Extraction of fitting parameters is performed with constant beam waists ω_0. For each receptor imaged and mouse type (wt vs TG32 or TG4) an average waist is calculated from MSD curves from the single cells along the plasma membrane. Each curve along the plasma membrane was fit to its extracted waist or determined from measuring fluorescent TetraSpec beads (ω_{bead} = 0.330 µm) where no waist could be extracted from the MSD plots (12). Across TTs the average waists from the scans along the plasma membrane were used except for β_2-AR for which the waist was taken from the TetraSpec beads.

The autocorrelation curves were normalized to their G(0) where possible. In case no correlation could be extracted, such as β_2-AR along the PM of CMs and in KO cells, the averaged G(0) at the TTs of the β_2-AR in wt CMs was taken for normalization.

Global linescan Spatio-Temporal Image Correlation Spectroscopy (STICS)
In case of STICS the spatio-temporal image correlations of these linescans are calculated removing any influence of photobleaching (8). The kymographs are corrected for drifts and slow fluctuations using a random number addition detrending within a moving window of approximately $250 \cdot 10^3$ lines (about 20 s) similar to (13). The spatiotemporal correlation curve is calculated (8).

$$G(\xi, \tau_i) = \frac{\langle \delta I(x, t_i) \cdot \delta I(x+\xi, t_i+\tau_i)\rangle}{\langle I(x, t_i)\rangle^2}$$

Where $\langle\rangle$ indicates the average over all positions x and scans i (corresponding to time t_i) and $\delta I(x, t_i) = I(x, t_i) - \langle I(x, t_i)\rangle$. ξ represents the spatial lag variable, t_i=iT the time and τ_i=iT the discrete time lag as an integer multiple of the scanning period. Alternatively, by calculating the fast Fourier transform (FFT) and its complex conjugate the autocorrelation or STICS function was determined by performing the inverse fast Fourier transform of the product of the two transforms (13).
The spatio-temporal correlation curve for pure diffusion in a 1-dimensional line scan can then be fitted to the following fitting model (8, 13):

$$G_{STICS}(\xi, \tau_i) = \frac{\gamma}{N\pi}\frac{1}{\omega_0^2 + 4D\tau_i}\, e^{\left(-\frac{\xi^2}{\omega_0^2+4D\tau_i}\right)}$$

Already simplified by elimination of the term of the line repetition rate which becomes negligible with increasing time lags. The diffusion coefficient D, the average number of particles in the observation volume N and the waist ω_0 can be obtained by fitting the equation to experimental data. γ represents a shape factor due to uneven illumination across the focal volume and is 0.3535 for a 3D Gaussian under ideal conditions (14).

Simulations of diffusion in T-tubules
We simulated diffusion on tubular geometries by direct numerical integration of the overdamped Langevin equation for every degree of freedom, $\dot{x}_i^n(t) = \sqrt{2D_i}\xi$ with ξ being normal Gaussian noise, n denoting the particle index and i identify the component of the positional vector (15). Here, we assume equal diffusivities for every particle, but explicitly allow for non-isotropic motility. Also,

it is noteworthy that such an analogous description is possible as the mantle surface of a cylinder can be mapped onto a planar rectangle (using an angle φ in circumferential direction and the distance h to some reference point in axial direction) with periodic boundary conditions. This way we move from Cartesian coordinates (*x,y,z*) with the constraint to be on the cylinder surface to the more suited, unconstrained coordinates (R,φ,h) with R being the radius of the tube.

Non-isotropic diffusivities allow us to simulate particles on a tubule with diffusion in only axial ($D_h \neq 0$, $D_\varphi = 0$, **Figure S3C** and center image A) or only circumferential ($D_h = 0$, $D_\varphi \neq 0$, **Figure S3D** and right image of A) direction and, thus, to disentangle their respective contributions to the autocorrelation function, particularly in scenarios where a closed analytical description might be hard to construct. Isotropic diffusivities allow us to simulate real data and extract the true diffusion coefficients (**Figure S3B**).

As we only consider freely diffusing particles on flat (in terms of their Gaussian curvature) membranes, the equilibrium distribution of particles is uniform with a particle density of 0.45 particles/μm^2 and we therefore initialize with random starting positions. Simulation parameters were chosen to reflect the real case with a tubular diameter of 175 nm (average diameter of 169 ± 15 nm (16)) and a diffusion constant of D= 0.1 $\mu m^2/s$.

General materials and methods for organic synthesis

Reagents and solvents were purchased in their purest grade from abcr, Acros, Alfa Aesar, Carbolution Chemicals, Jena Bioscience, Sigma Aldrich, TCI, VWR and were used without further purification. Unless otherwise noted, reactions were performed under nitrogen atmosphere employing dry solvents of commercial quality, used as purchased. All reactions were carried out using a magnetic stirrer. Solvents were evaporated by a rotary evaporator with a membrane vacuum pump. Products purified by preparative HPLC using aqueous solvents were lyophilized. TLC analyses were performed using Merck 60 F254 aluminum sheets and analyzed by UV light (254 nm). Purification by flash column chromatography was conducted using silica gel 60 (40-63 µm mesh, Merck) and eluents as binary mixtures with the volume ratios indicated. Preparative HPLC was performed on an Agilent 1200 preparative series HPLC system or on an Agilent HPLC 1260 Infinity system combined with an MWD detector and fraction collector, applying a linear gradient and a flow rate [FR] as indicated below. As HPLC column, a Zorbax-Eclipse XDB-C8 PrepHT (21.2 mm × 150 mm, 5 µm) was used. Compounds were characterized by NMR spectroscopy, IR spectroscopy, high-resolution mass spectra (HRMS) and purity was assessed by RP-HPLC. All assayed compounds were >95% pure. ESI-mass spectra were recorded using LC-MS: Thermo Scientific Dionex Ultimate 3000 UHPLC quarternary pump, autosampler and RS-diode array detector, column: Phenomenex Kinetex core shell analytical column, 2.1 mm × 75 mm, 2.6 µm, flow rate 0.3 mL/min, detection wavelength: 220 nm, coupled to a Bruker Daltonics Amazon mass spectrometer using ESI as ionization source. High mass accuracy and resolution experiments were performed on a Bruker Daltonics timsTOF Pro spectrometer using electrospray ionization (ESI) as ionization source or a Bruker Daltonik maXis 4G spectrometer using atmospheric pressure photoionization (APPI) as ionization source. NMR spectra were obtained either on a Bruker Avance III 400 or a Bruker Avance III 600 (600 MHz for ^1H and 151 MHz for ^{13}C) spectrometer, the latter equipped with a Prodigy nitrogen cooled probe at 297 K, using the deuterated solvents indicated below. For the spectra recorded in organic solvents, the chemical shifts are reported in ppm (δ) relative to TMS. For measurements in D_2O, the water peak was used for calibration. IR spectra were performed on a Jasco FT/IR 4100 spectrometer using a KBr pellet, as specified. Substance purities were assessed by analytical HPLC (Agilent 1100 analytical series, equipped with a quarternary pump and variable wavelength detector detector; column Zorbax Eclipse XDB-C8 analytical column, 4.6 mm × 150 mm, 5 µm, flow rate 0.5 mL/min, detection wavelengths: 220 nm, 254 nm, 280 nm and/or 655 nm). Linear gradient solvent systems were used as specified below.

Chiral analytical HPLC was run on a AGILENT series 1100 system equipped with a VWD and detection at 254 nm. As chiral column a DAICEL Chiralpak IC column (4.6 mm × 250 mm, 5 µM) was used at 20 °C and a flow rate 1.0 mL/min with the solvent system as indicated. Optical rotation values were obtained from a Jasco P2000 polarimeter with the solvents indicated. Melting points were determined in open capillaries using a Büchi 510 melting point apparatus and are given uncorrected.

Synthesis procedures

(*S*)-4-(Oxiran-2-ylmethoxy)-9*H*-carbazole (2) (1, 2)

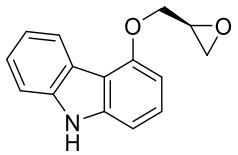

To a solution of 4-(oxiran-2-ylmethoxy)-9*H*-carbazole (**1**, 1000 mg, 5.46 mmol) in DMF (10 mL) was added a suspension of 60% sodium hydride in mineral oil (234 mg, 5.85 mmol, 1.07 eq) at 0 °C. After 30 min, the mixture was allowed warm to rt and then was added a solution of (*S*)-glycidyl 3-nitrobenzenesulfonate (1415 mg, 5.46 mmol) in DMF (5 mL). After 20 h, another portion of 60% sodium hydride in mineral oil (29 mg, 1.21 mmol, 0.2 eq) and (*S*)-glycidyl 3-nitrobenzenesulfonate (566 mg, 2.18 mmol, 0.4 eq) were added. After stirring for another 3 h, saturated aqueous NH_4Cl was added and extraction with *tert*-butyl methyl ether was performed. The organic layer was washed with 1N NaOH, dried with $MgSO_4$ and the solvent was evaporated. Flash chromatography (isohexane/ethyl acetate 9:1) furnished **2** (516 mg, 66%) as a beige solid, mp: 157 °C.

IR (KBr): 3295 cm^{-1}.

^1H NMR: (600 MHz, $CDCl_3$) δ 2.85 (dd, J = 5.1, 2.6 Hz, 1H), 2.94 (dd, J = 5.1, 4.3 Hz, 1H), 3.54 (dddd, J = 6.1, 4.3, 2.6, 2.6 Hz, 1H), 4.10 (dd, J = 11.2, 6.1 Hz, 1H), 4.56 (dd, J = 11.2, 2.6 Hz, 1H), 6.70 (d, J = 8.1 Hz, 1H), 7.10 (d, J = 8.1 Hz, 1H), 7.16 (ddd, J = 7.7, 7.1, 0.8 Hz, 1H), 7.30 (dd, J = 8.1, 8.1 Hz, 1H), 7.35 (dd, J = 8.0, 7.1 Hz, 1H), 7.46 (ddd, J = 8.0, 0.8, 0.7 Hz, 1H), 8.17 (d, J = 7.7 Hz, 1H), 11.27 (s, 1H).

ESI-MS: *m/z* 239.9 $[M+H]^+$

Chiral HPLC: isocratic elution with hexane/EtOH (+ 0.1% ethylenediamine) 9:1, **(*R*)-2** (t_R: 10.7 min): 0.8%, **(*S*)-2** (t_R: 14.8 min): 99.2%.

(9*H*-Fluoren-9-yl)methyl (4-nitrophenethyl)carbamate (4)

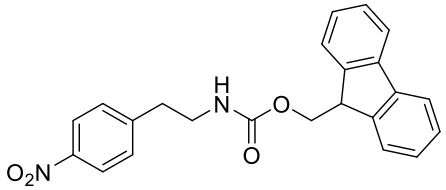

To a suspension of 2-(4-nitrophenyl)ethylamine-HCl (**3**, 1200 mg, 5.92 mmol) in CH_2Cl_2 (10 mL) was added DIEA (2296 mg, 3.2 mL, 17.76 mmol, 3 eq) and a solution of Fmoc-Cl (1838 mg, 7.11 mmol, 1.2 eq) in CH_2Cl_2 (10 mL) at 0 °C. The mixture was allowed warm to rt. After 2 h, the resulting

solution was washed with a saturated, aqueous solution of citric acid, dried with $MgSO_4$ and the solvent was evaporated. Flash chromatography (isohexane/ethyl acetate 3:1) and following crystallization after evaporation of the eluent furnished **4** (2300 mg, 66%) as a yellowish solid, mp: 123 °C.

IR (KBr): 3416, 3328, 1725, 1687 cm^{-1}.

^1H NMR: (600 MHz, $CDCl_3$, a 85:15 ratio of rotamers was observed) *δ* 2.51-2.62 and 2.86-2.96 (2× m, 2H), 3.08-3.20 and 3.42-3.59 (2× m, 2H), 4.16-4.25 (m, 1H), 4.42-4.51 (m, 2H), 4.60-4.68 and 4.71-4.79 (2× m, 2H), 7.10-7.12 and 7.27-7.36 (2× m, 4H), 7.38-7.43 (m, 2H), 7.51-7.61 (m, 2H), 7.72-7.80 (m, 2H), 8.07-8.19 (m, 2H).

^{13}C NMR: (DEPTQ, 151 MHz, $CDCl_3$) *δ* 36.2, 47.5, 66.6, 120.2, 124.0, 125.1, 127.2, 127.9, 129.9, 141.5, 144.0, 146.7, 147.0, 156.4

ESI-MS: *m/z* 389.1 $[M+H]^+$

HR-ESI-MS: *m/z* $[M+H]^+$ calcd. for $C_{23}H_{21}N_2O_4$: 389.1496, found 389.1494

(9*H*-Fluoren-9-yl)methyl (4-aminophenethyl)carbamate (5) (3, 4)

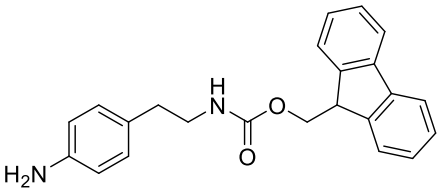

To a solution of (9*H*-fluoren-9-yl)methyl (4-nitrophenethyl)carbamate (**4**, 850 mg, 2.19 mmol) in DMF (3 mL) was added $SnCl_2 \times 2\ H_2O$ (2470 mg, 10.94 mmol, 5 eq). After stirring the mixture for 16 h at rt, the resulting solution was diluted with a saturated, aqueous solution of $NaHCO_3$, extracted with ethyl acetate and dried with $MgSO_4$. After evaporation of the solvent, the yellowish powder (**5**, 639 mg, 82%, mp: 136 °C) was used for the next reaction step without further purification.

IR (KBr): 3447, 3367, 3317, 1684 cm^{-1}.

^1H NMR: (600 MHz, $CDCl_3$, a 85:15 ratio of rotamers was observed) *δ* 2.23-2.30 and 2.48-2.57 (2× m, 2H), 2.85-2.93 and 3.07-3.15 (2× m, 2H), 4.15-4.23 (m, 1H), 4.25-4.31 and 4.38-4.45 (m, 2H), 4.84 (br s, 2H), 6.45-6.53 (m, 2H), 6.62-6.68 and 6.76-6.85 (2× m, 2H), 7.28-7.32 (m, 1H), 7.32-7.36 (m, 2H), 7.39-7.45 (m, 2H), 7.61-7.71 (m, 2H), 7.85-7.92 (m, 2H).

ESI-MS: *m/z* 359.1 $[M+H]^+$

HR-ESI-MS: *m/z* $[M+H]^+$ calcd for $C_{23}H_{23}N_2O_2$: 359.1754, found: 359.1753.

(9*H*-Fluoren-9-yl)methyl (4-(hex-5-ynamido)phenethyl)carbamate (6)

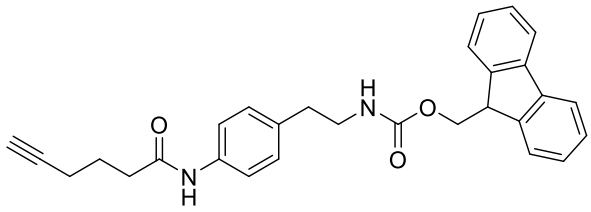

To a solution of hexynoic acid (188 mg, 190 μL,1.67 mmol) and HOAt (228 mg, 1.67 mmol, 1.2 eq) in a mixture of DMF (7 mL) and CH_2Cl_2 (5 mL) was added EDC × HCl (267 mg, 1.67 mmol, 1.2 eq). After stirring for 10 min at rt, a solution of of (9*H*-fluoren-9-yl)methyl (4-aminophenethyl)carbamate (**5**, 500 mg, 1.40 mmol) and DIEA (433 mg, 570 μL, 2.25 mmol, 2.4 eq) in CH_2Cl_2 (5 mL) was added. After 2 h, ethyl acetate (30 mL) was added and the resulting solution was washed successively with saturated, aqueous solutions of citric acid (3×), $NaHCO_3$ (3×) and NaCl (3×), dried with $MgSO_4$ and the volume of solvent was reduced to 25% by evaporation. The precipitate formed thereupon was collected by filtration and the filtrate was evaporated and subjected to flash chromatography (gradient isohexane/ethyl acetate 2:1 -> 1:1). Combining this fraction with the aforementioned precipitate gave **6** (435 mg, 69%) as a yellowish solid, mp: 174 °C.

IR (KBr): 3427, 3314, 1733, 1685 cm^{-1}.

^1H NMR: (600 MHz, $CDCl_3$, a 85:15 ratio of rotamers was observed) δ 1.75 (tt, J = 7.3, 7.1 Hz, 2H), 2.22 (td, J = 7.1, 2.7 Hz, 2H), 2.32-2.38 and 2.63-2.68 (2× m, 2H), 2.40 (t, J = 7.3 Hz, 2H), 2.81 (t, J = 2.7 Hz, 2H), 2.90-2.97 and 3.15-3.21 (2× m, 2H), 4.18-4.25 (m, 1H), 4.26-4.31 and 4.39-4.45 (2× m, 2H), 6.80-6.90 and 7.07-7.11 (2× m, 2H), 7.30-7.37 (m, 3H), 7.39-7.44 (m, 2H), 7.47-7.55 (m, 2H), 7.60-7.69 (m, 2H), 7.86-7.92 (m, 2H), 9.95 (s, 1H).

^{13}C NMR: (151 MHz, $CDCl_3$) δ 17.3, 23.9, 34.7, 35.0, 41.8, 46.7, 65.1, 71.5, 84.0, 119.0, 120.0, 125.1, 127.0, 127.5, 128.7, 133.8, 137.3, 140.7, 143.9, 155.9, 170.3.

ESI-MS: *m/z* 453.2 $[M+H]^+$.

HR-APPI-MS: *m/z* $[M+H]^+$ calcd. for $C_{29}H_{28}N_2O_3$: 453.2173, found: 453.2171.

HPLC: linear gradient 3–85% CH_3CN in H_2O (+ 0.1% TFA) in 0-26 min, t_R = 24.9 min, purity: >99%

_N_-(4-(2-Aminoethyl)phenyl)hex-5-ynamide (7)

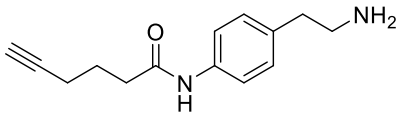

To a solution of (9*H*-fluoren-9-yl)methyl (4-(hex-5-ynamido)phenethyl)carbamate (**6**, 435 mg, 0.96 mmol) in DMF (2 mL) was added 1,8-diazabicyclo[5.4.0]undec-7-ene (DBU, 1462 mg, 9.61 mmol, 10 eq). After stirring for 2 h at rt, the solvent was evaporated. Flash chromatography (gradient CH_2Cl_2/MeOH 95:5 -> 90:10) afforded **7** (154 mg, 70%) as a white solid, mp: 176 °C.

IR (KBr): 3303, 3286, 1662 cm^{-1}.

^1H NMR: (600 MHz, $CDCl_3$) δ 1.75 (tt, J = 7.4, 7.2 Hz, 2H), 2.21 (td, J = 7.2, 2.6 Hz, 2H), 2.40 (t, J = 7.4 Hz, 2H), 2.65-2.68 (m, 2H), 2.81 (t, J = 2.6 Hz, 2H), 2.81-2.84 (m, 2H), 7.10-7.15 (m, 2H), 7.48-7.53 (m, 2H), 9.92 (s, 1H).

^{13}C NMR: (151 MHz, $CDCl_3$) δ 17.4, 24.0, 35.0, 36.5, 42.2, 71.6, 84.0, 119.2, 128.8, 133.7, 137.5, 170.4.

ESI-MS: *m/z* 231.0 $[M+H]^+$.

HR-ESI-MS: *m/z* $[M+H]^+$ calcd. for $C_{14}H_{19}N_2O$: 231.1492, found: 231.1493.

HPLC: linear gradient 3–50% CH_3CN in H_2O (+ 0.1% TFA) in 0-15 min, t_R = 12.5 min, purity: >99%

(*S*)-*N*-(4-(2-((3-((9*H*-Carbazol-4-yl)oxy)-2-hydroxypropyl)amino)ethyl)phenyl)hex-5-ynamide × TFA (8)

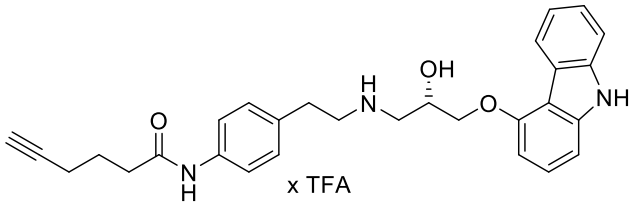

A solution of (*S*)-4-(oxiran-2-ylmethoxy)-9*H*-carbazol (**2**, 5.0 mg, 0.021 mmol) and *N*-(4-(2-aminoethyl)phenyl)hex-5-ynamide (**7**, 6.1 mg, 0.027 mmol, 1.3 eq) in isopropanol (1 mL) was heated for 5 h in a sealed tube using an oil bath at 85 °C. After evaporation of the solvent, the residue was purified by preparative HPLC (FR: 12 mL/min) applying a linear gradient 3–50% CH_3CN in H_2O (+ 0.1% TFA) in 0-15 min (t_R: 14.9 min) to afford **8** (10.6 mg, 86%, M_r: 583.26) as a white solid, mp: 79-80 °C.

IR (KBr): 3407, 3294, 1676 cm^{-1}.

^{1}H NMR: (600 MHz, $CDCl_3$) δ 1.75 (tt, *J* = 7.1, 7.1 Hz, 2H), 2.23 (td, *J* = 7.1, 2.6 Hz, 2H), 2.40 (t, *J* = 7.1 Hz, 2H), 2.81 (t, *J* = 2.6 Hz, 1H), 2.88-2.98 (m, 2H), 3.18-3.26 (m, 3H), 3.34-3.38 (m, 1H), 4.18-4.22 (m, 1H), 4.23-4.26 (m, 1H), 4.35-4.43 (m, 1H), 6.01 (brs, 1H), 6.71 (*J* = 8.0 Hz, 1H), 7.10 (d, *J* = 8.0 Hz, 1H), 7.14 (ddd, *J* = 7.9, 7.1, 1.1 Hz, 1H), 7.17-7.20 (m, 2H), 7.31 (dd, *J* = 8.0, 8.0 Hz, 1H), 7.35 (ddd, *J* = 8.3, 7.1, 0.9 Hz, 1H), 7.46 (d, *J* = 8.3 Hz, 1H), 7.53-7.56 (m, 2H), 8.22 (d, *J* = 7.9 Hz, 1H), 8.68 (brs, 1H), 9.92 (s, 1H), 11.29 (s, 1H).

^{13}C NMR: (151 MHz, $CDCl_3$) δ 17.8, 24.4, 31.5, 35.5, 48.8, 50.2, 65.7, 70.2, 72.1, 84.5, 101.0, 104.8, 110.9, 112.0, 119.1, 119.8, 122.0, 123.0, 125.1, 126.9, 129.4, 132.1, 138.5, 139.4, 141.7, 155.0, 171.0.

ESI-MS: *m/z* 470.2 $[M+H]^+$.

HR-ESI-MS: *m/z* $[M+H]^+$ calcd. for $C_{29}H_{32}N_3O_3$: 470.2438, found: 470.2439.

$[\alpha]_D^{25}$: - 23.2 ° (c = 0.15 in methanol)

HPLC: linear gradient 3–65% CH_3CN in H_2O (+ 0.1% HCO_2H) in 0-26 min, t_R = 19.7 min, purity: >99%

Chiral HPLC: isocratic elution with hexane/EtOH (+ 0.1% ethylenediamine) 8:2, **(*R*)-8** (t_R: 11.6 min): 1.7%, **(*S*)-8** (t_R: 14.4 min): 98.3%.

1-(6-((3-(4-(4-((4-(2-(((*S*)-3-((9*H*-Carbazol-4-yl)oxy)-2-hydroxypropyl)amino)ethyl)phenyl)amino)-4-oxobutyl)-1*H*-1,2,3-triazol-1-yl)propyl)amino)-

6-oxohexyl)-2-((1*E*,3*E*)-5-((*E*)-3,3-dimethyl-5-sulfo-1-(3-sulfopropyl)indolin-2-ylidene)penta-1,3-dien-1-yl)-3-methyl-3-(4-sulfobutyl)-3*H*-indol-1-ium-5-sulfonate × TFA (JE1319)

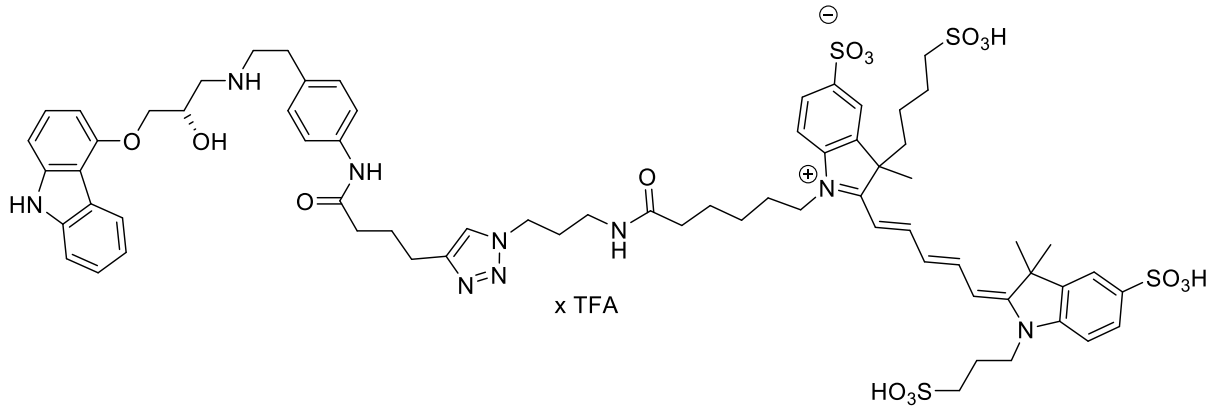

Remark: Stock solutions of all reaction components were prepared. Prior to the preparation of the stock solutions, all solvents were degassed by evaporation and, subsequently, flushed with nitrogen. The reaction sample and the product were protected against light exposure. A 0.1 M solution of HEPES buffer pH 7.5 was used.

To a solution of copper sulfate pentahydrate (0.20 mg, 0.79 µmol) in H_2O (150 µL) was added a solution of tris(3-hydroxypropyltriazolylmethyl)amine (THPTA, 1.7 mg, 3.9 µmol) in HEPES buffer (150 µL) and subsequently sodium ascorbate (3.9 mg, 19.7 µmol) in HEPES buffer (150 µL). To this solution, a solution of the Alexafluor 647 derivative AF 647 azide (Jena Bioscience, 0.5 mg, 0.53 µmol) in HEPES buffer (100 µL) and after 3 min a solution of **8** (1.20 mg, 2.1 µmol) in methanol (200 µL) was added. After 10 min of gentle agitation, the resulting solution was purified by preparative HPLC (FR: 12 mL/min, single injection of the *complete* sample) applying a linear gradient 3–50% CH_3CN in H_2O (+ 0.2% TFA) in 0-15 min (t_R: 11.0 min). The reaction was repeated under the same conditions and the collected product peaks of the two consecutive reactions (with 1 mg AF 647 azide in total) were combined and lyophilized to afford **JE1319** (0.8 mg, 50%, M_r: 1538.75) as a dark blue solid.

^{1}H NMR: (600 MHz, D_2O) δ 0.32-0.48 (m, 1H), 0.60-0.73 (m, 1H), 0.76-0.86 (m, 1H), 0.92-1.09 (m, 2H), 1.10-1.52 (m, 18H), 1.72-2.07 (m, 10H), 2.18-2.35 (m, 2H), 2.46-2.52 (m, 2H), 2.74-2.80 (m, 2H), 2.82-2.97 (m, 4H), 3.03-3.20 (m, 4H), 3.42-3.69 (m, 2H), 3.71-4.07 (m, 3H), 4.09-4.33 (m, 2H), 5.70-5.87 (m, 1H), 5.87-5.99 (m, 1H), 6.11-6.24 (m, 1H), 6.34-6.47 (m, 1H), 6.72-7.21 (m, 10H), 7.22-7.35 (m, 1H), 7.50-7.79 (m, 7H), 7.80-7.94 (m, 1H).

ESI-MS: *m/z* 712.8 $[M+2H]^{2+}$.

HR-ESI-MS: *m/z* $[M+2H]^{2+}$ calcd. for $C_{69}H_{87}N_9O_{16}S_4$: 712.7573, found: 712.7571.

HPLC: linear gradient 3–50% CH_3CN in H_2O (+ 0.1% TFA) in 0-15 min, t_R = 13.2 min, purity: 97.8%

Radioligand binding studies.

Binding affinities towards the human β_1 and β_2 receptors were determined as described previously(2, 17). Cell-based determination of binding affinity was performed with HEK293T cells transiently transfected with β_1-AR or β_2-AR (cDNA for β_1-AR provided by R. Sunahara, UCSD or β_2-AR obtained from the cDNA resource center, www.cdna.org). Two days after transfection, cells

were harvested and diluted in binding buffer to a final number of cells of 10,000 cells/well for β_1-AR and 50,000-100,000 cells/well for β_2-AR and competition binding experiments were performed as described above at a radioligand concentration of 0.2 nM [^{3}H]CGP 12,177. Non-specific binding was determined in the presence of unlabeled CGP 12,177 at a final concentration of 10 µM. Receptor densities (B_{max} value in fmol/cells) and specific binding affinities for [^{3}H]CGP 12,177 (K_D value) were determined as 9.6 ± 0.25 fmol/10^3 cells and 0.59 ± 0.063 nM for β_1-AR and 0.85 ± 0.043 pmol/cell and 0.45 ± 0.023 nM for β_2-AR, respectively. K_D and B_{max} values are derived from four individual experiments. K_D values are calculated without correction of radioligand depletion.
The resulting competition curves were analyzed by nonlinear regression using the algorithms implemented in PRISM 8.0 (GraphPad Software, San Diego, CA) to provide an IC_{50} value, which was subsequently transformed into a K_i value employing the equation of Cheng and Prusoff (19). Mean K_i values (±SEM) were derived from two (β_1-AR) or eight (β_2-AR) individual experiments based on cells, each performed in triplicates.

Supplementary Figures

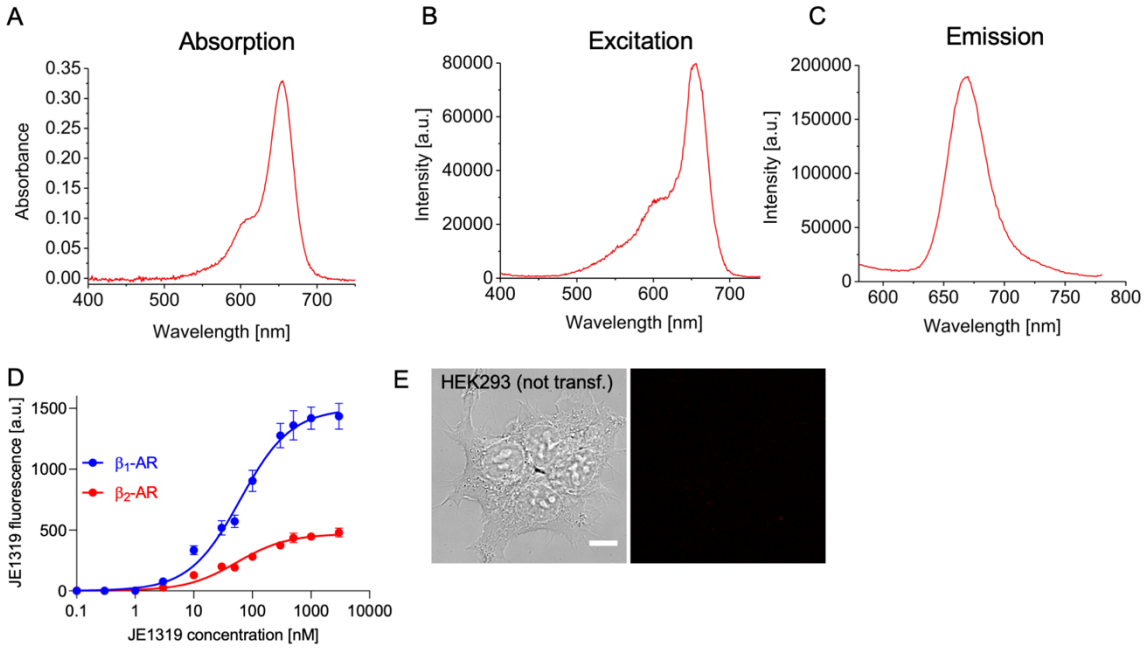

Figure S1: **Further properties of ligand JE1319**. (A-C) Absorption, excitation and emission spectra. (D) Saturation curves for JE1319 binding to intact HEK293 cells, overexpressing the β_1-AR-CFP or the mTurquoise2-β_2-AR (n=2 transfections, 8 individual experiments), measured in a 96-well plate reader geometry, yielding K_D-values of 62 ± 7 nM and 54 ± 9 nM respectively. Error is SEM (E) DIC and - confocal fluorescence images of untransfected HEK293AD incubated with 5 nM JE1319 as in Figure 1. Scale bar is 10 µm. (n=2 imaging sessions).

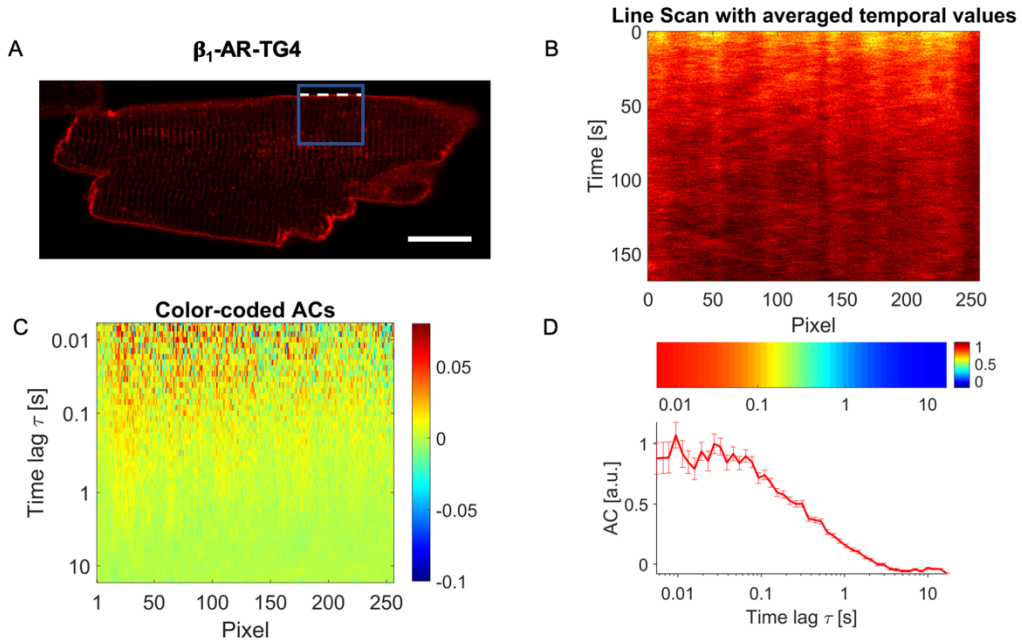

Figure S2: **Pixel by pixel analysis of linescans** (A) Example image of a β_1-AR-TG4 cell stained with 5 nM JE1319 in the presence of 50 nM ICI 118,551. Box highlights ROI and line which is scanned either 303,104 or 507,904 times with a frequency of 1,800 Hz. Scale bar is 20 µm. (B) Shows the intensities of each pixel over time. For illustration purposes multiple time points are averaged together to display 500 time points in the kymograph in a red-hot color scale. (C) Map of the autocorrelations. (D) Averaging of the autocorrelations from the selected portions in C into one row of the map. The chart below shows the averaged, normalized autocorrelation curve. Error bars indicate SEM

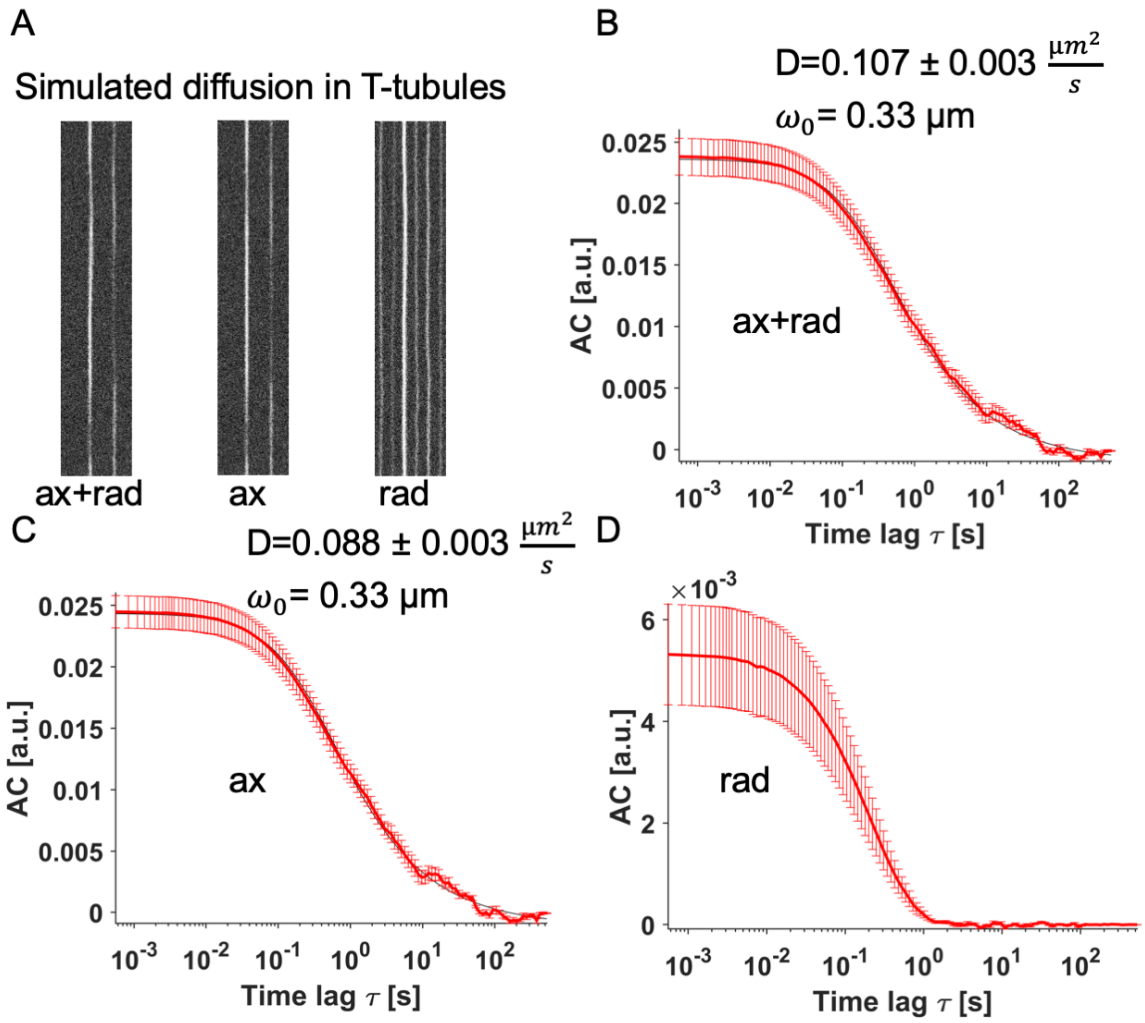

Figure S3: **Simulation of diffusion in T-tubules.** (A): Left to right shows simulated kymographs (200 pixels, 1000 time points displayed, 1800 Hz scan rate) of both axial and circumferential (or radial), - only axial and - only radial diffusion. (B-D) Autocorrelation curve of both axial and radial (B), (C) only axial and (D) only radial diffusion. There is no simple closed form for the autocorrelation curve for radial (circumferential) diffusion, but the timescale of de-correlation in this geometry is given by $T_d=d^2/D$ ~ 0.3 s in line with what is observed. Diameter of the simulated TTs is 175 nm. Simulated PSF waist and diffusion constant were ω_0=0.33 μm and D=0.1 μm^2/s. Error bars indicate SEM

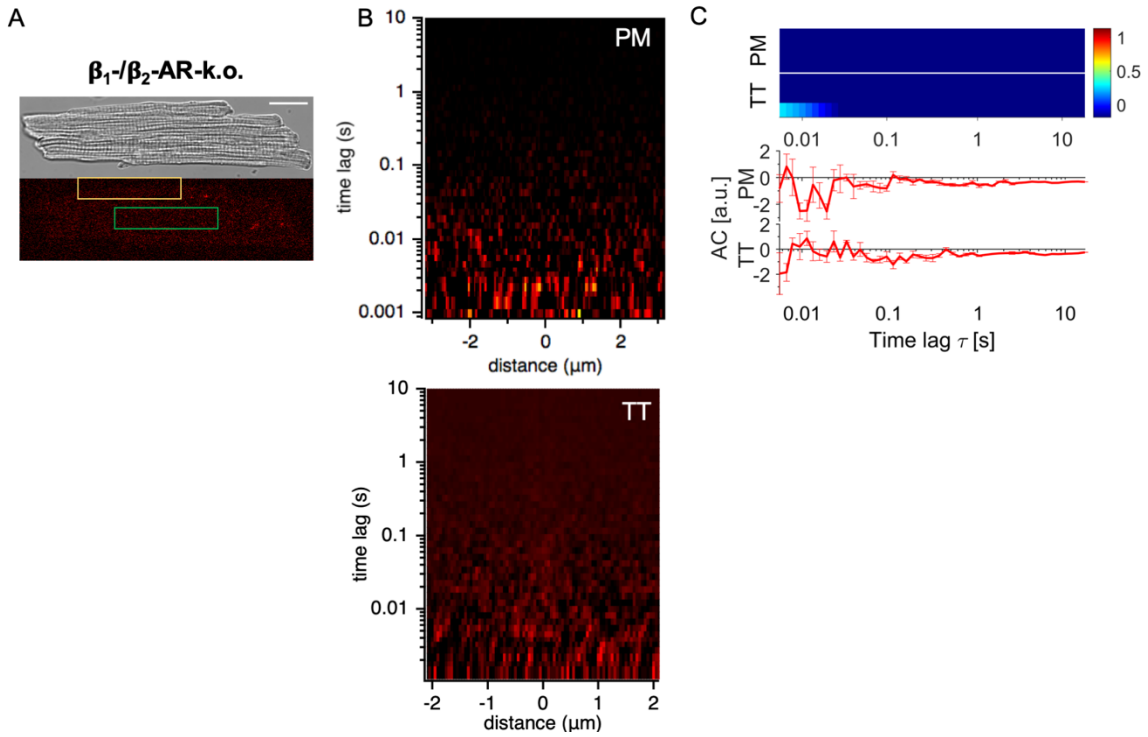

Figure S4: β1-AR/β2-AR-knockout cardiomyocytes show no diffusion of β-ARs neither along the outer plasma membrane nor on T-tubules, with 5 nM JE1319 labelling. (A) Image of an adult CM of a β1-AR/β2-AR-k.o. mouse (contrast set to 0). Scale bar is 20 µm. (B) Example of STICS functions of a β1/ β2-k.o. cell. (top) Plasma membrane (bottom) T-tubules (C) Normalized autocorrelation curves of β1-AR/β2-AR-k.o. cells. Autocorrelation curves along the PM and TTs (3 cells each, 1 mouse) are collected together in one plot separated by a white line. Each row represents the autocorrelation curve of one cell. For TT measurements each row represents the average of 6-7 tubules. The bottom chart depicts the corresponding autocorrelation (AC) functions. Error bars indicate SEM.

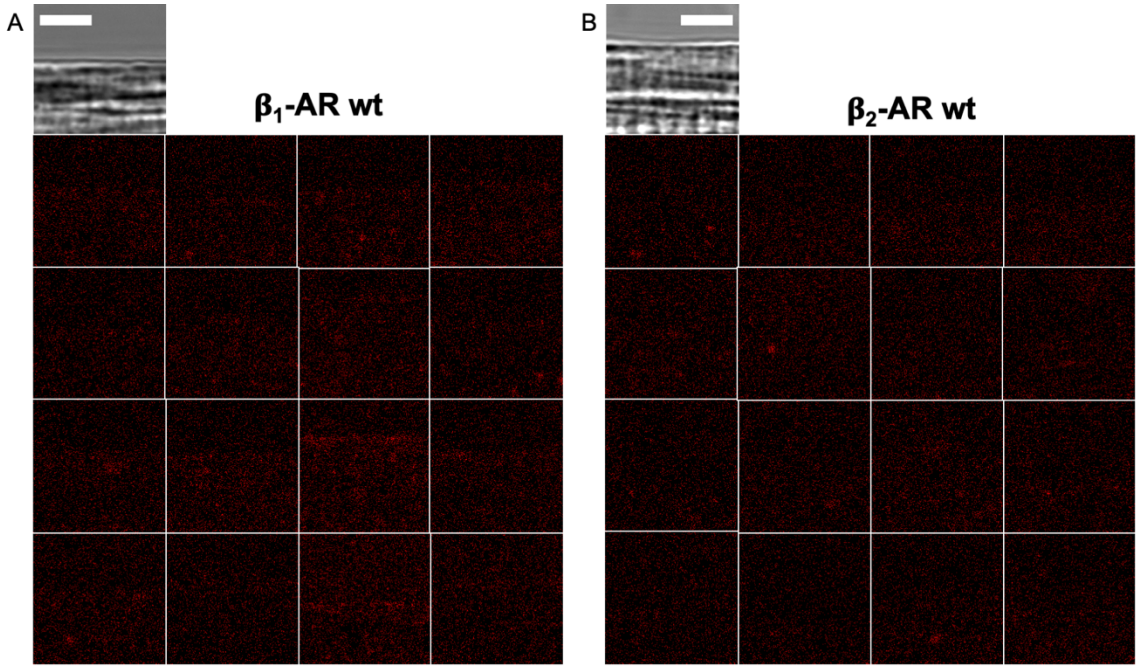

Figure S5: Representative fluorescence intensity mosaics of the outer plasma membrane wild type cardiomyocytes labelled with 50 nM JE1319. (A) Regions of the plasma membrane of wt CMs where β_1- and (B) β_2-AR were respectively stained and imaged at slow speed (10 Hz) at the confocal microscope. Each tile of the mosaic represents one cell. The area shown corresponds to the outer plasma membrane, as highlighted by the representative DIC image on the top. Scale bars are 5 µm. Contrast is set to 0. Excitation: 633 nm. Detection: 650 nm-750 nm. Receptors are labelled with 50 nM JE1319 and pre-treated with 50 nM ICI 118,551 (A) or 100 nM CGP 20712 (B).

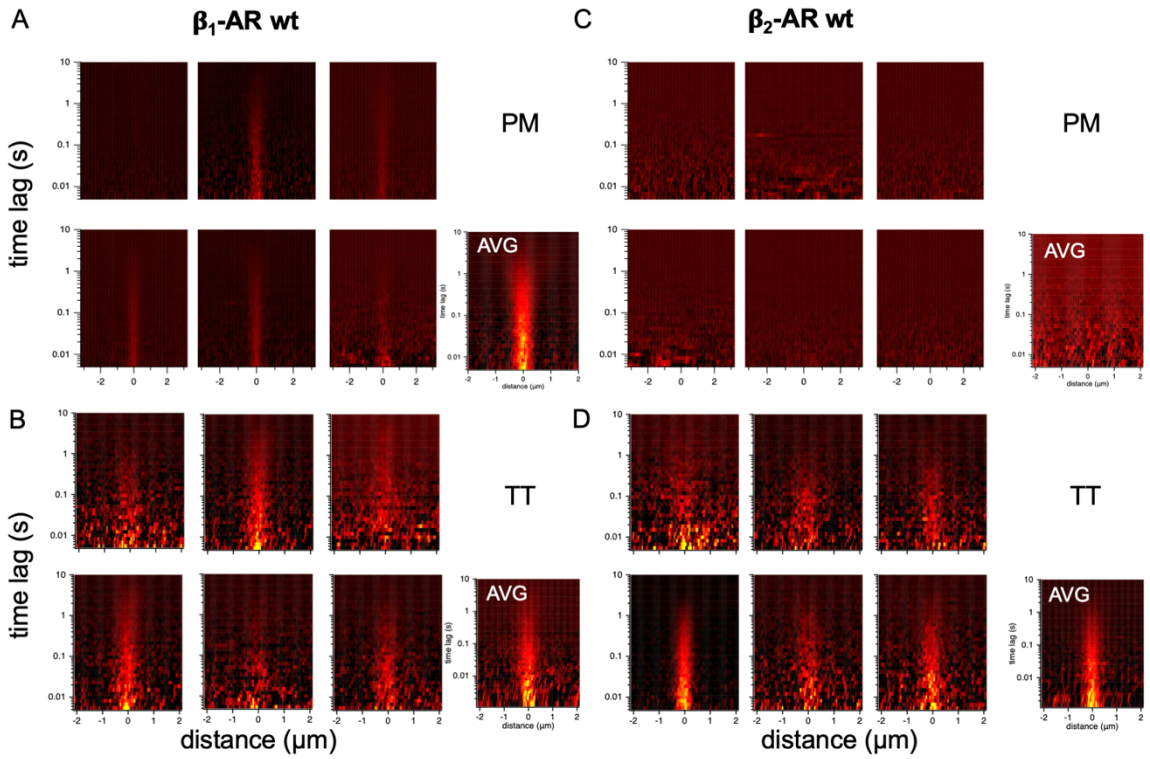

Figure S6: Representative diffusion mosaics of wild type cardiomyocytes along the plasma membrane and T-Tubules, labelling with 50 nM JE1319. Panels show STICS functions of labelled β_1- (A,B) and β_2-AR (C,D) in adult wild type cardiomyocytes, respectively on the PM (A,C) and TT (B,D). Each map in the panels represents the result from the analysis of 1 cell. Average STICS functions are displayed on the side. Receptors are labelled with 50 nM JE1319 and pre-treated with 50 nM ICI 118,551 (A,B) and 100 nM CGP 20712 (C,D).

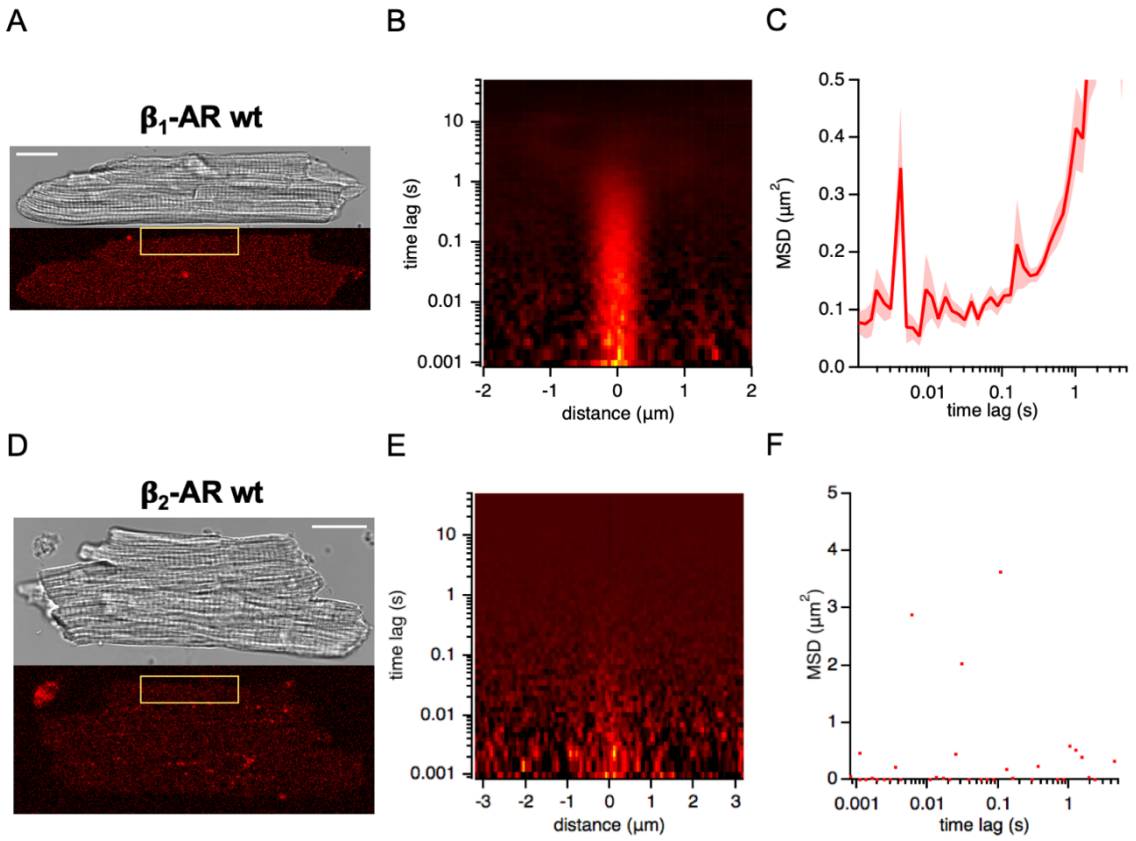

Figure S7: Diffusion of β-AR in wild type cardiomyocytes along the outer plasma membrane, labelling with 5 nM JE1319. (A) Image of an adult wild type cardiomyocyte with labelled β_1-AR. Receptors are labelled with 5 nM JE1319 and pre-treated with 50 nM ICI 118,551. Contrast is set to 0. (B) Representative STICS function for β_1-AR diffusion along the membrane of the cardiomyocyte. (C) Average MSD curve between 1 ms and 5 s extracted from n=6 cardiomyocytes (2 mice). Shading indicates SEM D-F same as in A-C for labelled β_2-AR, i.e. after pre-treatment with 100 nM CGP 20712 (n=6 cardiomyocytes, 1 mouse). Scale bars are 20 μm.

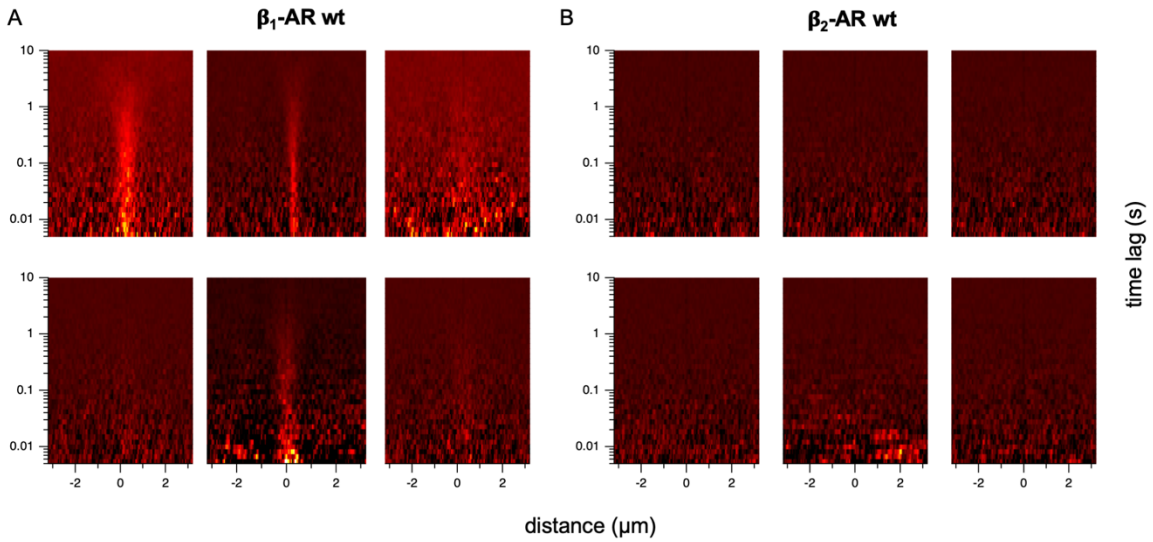

Figure S8: Diffusion mosaics of wild type cardiomyocytes along the plasma membrane, labelling with 5 nM JE1319. (A) STICS function of adult wild type cardiomyocytes stained for β_1- and (B) β_2-AR. Each STICS function in the panels represents the result from the analysis of one cell. Receptors are labelled with 5 nM JE1319 and pre-treated with 50 nM ICI 118,551 (A) or 100 nM CGP 20712 (B).

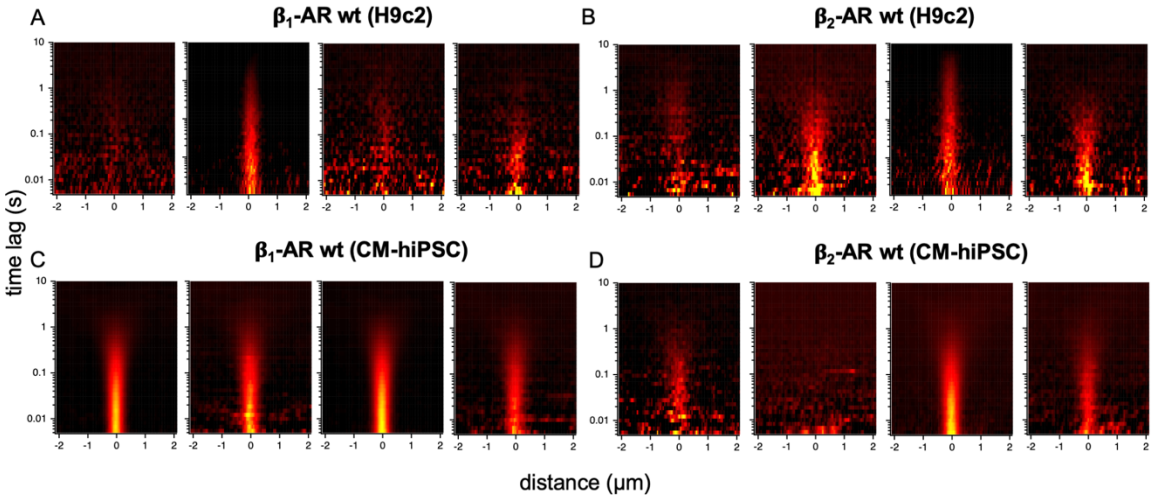

Figure S9: Diffusion mosaics of H9c2 and CM-hiPSC PM, labelling with 50 nM JE1319. (A) STICS functions of H9c2 cells stained for β_1- and (B) β_2-AR. (C) STICS functions of CM-hiPSCs cultured for 107 days and stained for β_1- and (D) β_2-AR. Each STICS function in the panels represents the result from the analysis of one cell. Receptors are labelled with 50 nM JE1319 and pre-treated with 50 nM ICI 118,551 (A,C) or 100 nM CGP 20712 (B,D).

SI References

1. E. A. Dubois *et al.*, Synthesis and in Vitro and in Vivo Characteristics of an Iodinated Analog of the β-Adrenoceptor Antagonist Carazolol. *J. Med. Chem.* **39**, 3256-3262 (1996).
2. M. Stanek *et al.*, Hybridization of β-Adrenergic Agonists and Antagonists Confers G Protein Bias. *J. Med. Chem.* **62**, 5111-5131 (2019).
3. S. Hou, X.-L. Sun, C.-M. Dong, E. L. Chaikof, Facile Synthesis of Chain-End Functionalized Glycopolymers for Site-Specific Bioconjugation. *Bioconjugate Chem.* **15**, 954-959 (2004).
4. A. Walia, S. Kang, R. B. Silverman, Microwave-Assisted Protection of Primary Amines as 2,5-Dimethylpyrroles and Their Orthogonal Deprotection. *J. Org. Chem.* **78**, 10931-10937 (2013).
5. V. Hong, S. I. Presolski, C. Ma, M. G. Finn, Analysis and Optimization of Copper-Catalyzed Azide-Alkyne Cycloaddition for Bioconjugation. *Angew. Chem., Int. Ed.* **48**, 9879-9883, S9879/9871-S9879/9810 (2009).
6. R. Nolan (2018) Algorithms for the Correction of Photobleaching. (Oxford).
7. E. L. Elson, D. Magde, Fluorescence correlation spectroscopy. I. Conceptual basis and theory. *Biopolymers* **13**, 27 (1974).
8. J. Ries, S. Chiantia, P. Schwille, Accurate determination of membrane dynamics with line-scan FCS. *Biophysical Journal* **96**, 2008 (2009).
9. M. Radek, M. Hof (Fluorescence Correlation Spectroscopy (FCS).
10. E. Haustein, P. Schwille, Fluorescence correlation spectroscopy: novel variations of an established technique. *Annu Rev Biophys Biomol Struct* **36**, 151-169 (2007).
11. Y. Jiang, A. Melnykov, E. Elson, FCS in closed systems and application for membrane nanotubes. *bioarXiv*, 134742 (2017).
12. M. Bathe-Peters, P. Gmach, P. Annibale, M. J. Lohse, Linescan microscopy data to extract diffusion coefficient of a fluorescent species using a commercial confocal microscope. *Data in Brief* **29**, 105063 (2020).
13. C. Di Rienzo, E. Gratton, F. Beltram, F. Cardarelli, Fast spatiotemporal correlation spectroscopy to determine protein lateral diffusion laws in live cell membranes. *Proc Natl Acad Sci U S A* **110**, 12312 (2013).
14. C. M. Brown *et al.*, Raster image correlation spectroscopy (RICS) for measuring fast protein dynamics and concentrations with a commercial laser scanning confocal microscope. *Journal of Microscopy* **229**, 91 (2008).
15. N. G. van Kampen, *Stochastic Processes in Physics and Chemistry* (1992), vol. 1.
16. C. H. T. Kong, E. A. Rog-Zielinska, C. H. Orchard, P. Kohl, M. B. Cannell, Sub-microscopic analysis of t-tubule geometry in living cardiac ventricular myocytes using a shape-based analysis method. *Journal of Molecular and Cellular Cardiology* **108**, 7 (2017).
17. H. Hubner *et al.*, Structure-guided development of heterodimer-selective GPCR ligands. *Nat Commun* **7**, 12298 (2016).
18. O. H. Lowry, N. J. Rosebrough, A. L. Farr, R. J. Randall, Protein measurement with the Folin phenol reagent. *J Biol Chem* **193**, 265-275 (1951).
19. Y. Cheng, W. H. Prusoff, Relationship between the inhibition constant (K1) and the concentration of inhibitor which causes 50 per cent inhibition (I50) of an enzymatic reaction. *Biochem Pharmacol* **22**, 3099-3108 (1973).